The Dimensional Hierarchy of Cortical Oscillations: From Analog Substrate to Symbolic Codes

Ian Todd

Sydney Medical School, University of Sydney

`itod2305@uni.sydney.edu.au`

November 28, 2025

Abstract

We propose that cortical oscillations implement a *dimensional hierarchy*: a cascade of progressively tighter information bottlenecks from slow to fast frequencies. Using graph Laplacian analysis, we show that slow eigenmodes engage substantially more oscillators than fast modes ($r = -0.75$), establishing the high-dimensional geometric substrate. Using encoder-decoder networks, we show that discrete symbolic codes emerge at a critical bottleneck width of $k = 2$, while $k = 3$ preserves continuous "floppy" dynamics capable of representing self-referential structures without trajectory collision. We argue that this hierarchy maps onto frequency bands: slow oscillations maintain the volumetric analog context; beta ($k \approx 3$) supports manipulation and meta-cognition; gamma ($k \approx 2$) forces categorical commitment. The capacity to sustain $k \geq 3$ dynamics—to hold contradictions without collapsing them—may be a geometric signature of cognitive and emotional maturity. Long-wavelength oscillations provide the temporal stability and geometric depth required for collision-free representations; their disruption forces premature discretisation.

1 Introduction

1.1 The Dimensionality Question

Influential work on oscillatory dynamics in prefrontal cortex suggests that different frequency bands serve distinct computational roles (Miller et al., 2018; Lundqvist et al., 2016). Low-frequency oscillations are often characterised as "low-dimensional" coordinating signals, while gamma activity is associated with "high-dimensional" information processing (Bastos et al., 2015).

However, this framing conflates two distinct notions of dimensionality:

1. **Temporal complexity**: How many independent time-varying components describe the signal at a single site.

2. **Geometric dimensionality**: How many degrees of freedom participate coherently across space.

A slow wave sweeping across cortex may appear "simple" at a single electrode but coordinates thousands of oscillators into coherent phase relationships (high geometric dimensionality). Conversely, a gamma burst may exhibit complex temporal structure but engage only a small cortical population (low geometric dimensionality).

1.2   The Hierarchy Hypothesis

We propose that the frequency spectrum implements a *dimensional hierarchy*—a cascade of information bottlenecks:

Band	Bottleneck	Topology	Function
Delta/Theta	$k \gg 3$	Volumetric	Raw substrate
Beta	$k \approx 3$	Floppy manifold	Manipulation, meta-cognition
Gamma	$k \approx 2$	Discrete clusters	Symbols, decisions

The key insight is that **different bottleneck widths support qualitatively different computations**. At $k = 2$, the system is forced to discretise—continuous manifolds collapse into distinct attractor basins ("symbols"). At $k \geq 3$, the system retains enough dimensionality to represent continuous processes, including self-referential structures that would produce trajectory collisions in lower dimensions.

1.3   Maturity as Dimensional Capacity

We further speculate that the capacity to sustain $k \geq 3$ dynamics—to hold contradictions, ambiguity, and nuance without forcing premature resolution—constitutes a geometric signature of cognitive and emotional maturity. The immature or stressed mind collapses to $k = 2$: black/white, good/bad, us/them. The mature mind can inhabit the "floppy" space where paradoxes coexist.

Long-wavelength (slow) oscillations provide the *temporal stability* required for collision-free representations. When slow-wave power is reduced (stress, sleep deprivation, developmental immaturity), the system loses the substrate needed to maintain $k \geq 3$ dynamics and defaults to rigid categorical processing.

2   Methods

2.1   Laplacian Eigenmodes and Participation Ratio

2.1.1   Network Construction

We model cortical connectivity using a modular (stochastic block) network with $N = 2500$ nodes organised into 25 modules of 100 nodes each. Connection probability within modules was $p_{\text{within}} = 0.3$; between modules, $p_{\text{between}} = 0.01$.

The unnormalised graph Laplacian L has diagonal entries equal to node degree and off-diagonal entries of -1 for each edge:

$$L_{ij} = \begin{cases} \deg(i) & \text{if } i = j \\ -1 & \text{if } i \sim j \\ 0 & \text{otherwise} \end{cases} \tag{1}$$

2.1.2   Participation Ratio

For a normalised eigenmode ψ across N oscillators:

$$\text{PR}(\psi) = \frac{1}{\sum_i |\psi_i|^4}, \quad \text{with } \sum_i |\psi_i|^2 = 1. \tag{2}$$

$\text{PR} \approx N$ when all oscillators contribute equally; $\text{PR} \approx 1$ when activity is confined to a single oscillator. We computed the 150 smallest eigenpairs using ARPACK.

2.1.3 Synthetic Time-Series Validation

To verify that the participation ratio metric correctly distinguishes global from local activity in time-series data, we generated synthetic multi-channel signals. Slow activity (2–8 Hz) was simulated as a global oscillation with high inter-channel correlation ($r = 0.8$); fast activity (30–50 Hz) was simulated as sparse, uncorrelated bursts. The combined signal was bandpass filtered and PR was computed on amplitude envelopes over 200 ms sliding windows. This establishes that PR correctly identifies global versus local activity when the spatial structure is uncontaminated by volume conduction.

2.2 Bottleneck Compression

2.2.1 Category Construction

We defined six categories as smooth phase gradient patterns across 256 oscillators:

$$\phi_c(i) = 0.3 \cos(x_i + \theta_c) + 0.2 \sin(0.5 x_i + \theta_c) \tag{3}$$

where $x_i \in [0, 4\pi]$ and $\theta_c = \pi c/6$. Samples were generated by adding Gaussian noise ($\sigma = 0.5$), yielding 200 samples per category.

2.2.2 Network Architecture

The encoder-decoder compresses 256-D input through bottlenecks of width $k \in \{1, 2, 3, 4, 8, 16, 32\}$:

- **Encoder**: $256 \to 128 \to 128 \to k$ (ReLU)

- **Bottleneck**: k dimensions with additive Gaussian noise ($\sigma = 0.5$)

- **Decoder**: $k \to 128 \to 128 \to 256$ (ReLU)

Training used Adam ($\text{lr} = 10^{-3}$) for 150 epochs, minimising MSE reconstruction error. Code formation was measured by Adjusted Rand Index (ARI) between k-means clustering of bottleneck codes and true labels.

2.3 Paradox Topology Simulation

To demonstrate collision dynamics, we simulated a self-referential process (the Liar's Paradox: TRUE $\to$ FALSE $\to$ TRUE $\to$ ...) as a continuous trajectory and embedded it in 2D versus 3D spaces:

- **2D embedding**: The cyclic trajectory must trace a closed loop, producing self-intersections ("collisions") at every cycle.

- **3D embedding**: The trajectory can spiral upward (helix), with time as the third dimension, avoiding self-intersection.

Self-intersections were counted as pairs of trajectory points that are spatially close (< 0.15 units) but temporally distant (> 10 steps apart).

3 Results

3.1 Slow Modes Have Higher Participation

Figure 1 shows participation ratio versus normalised eigenvalue. There is a strong negative correlation ($r = -0.75$, $p < 0.001$): slower modes engage substantially more oscillators. The slowest 15 modes have mean PR $\approx$ 560 (23% of nodes); the fastest 15 modes have mean PR $\approx$ 175 (7% of nodes)—a 3-fold difference.

Synthetic time-series validation (Figure 2) confirms that PR correctly distinguishes global from local activity. Slow-band activity (2–8 Hz) engaged 99% of channels (PR = 63.2/64); fast-band activity (30–50 Hz) engaged only 42% (PR = 26.6/64)—a 2.4-fold difference matching the Laplacian prediction.
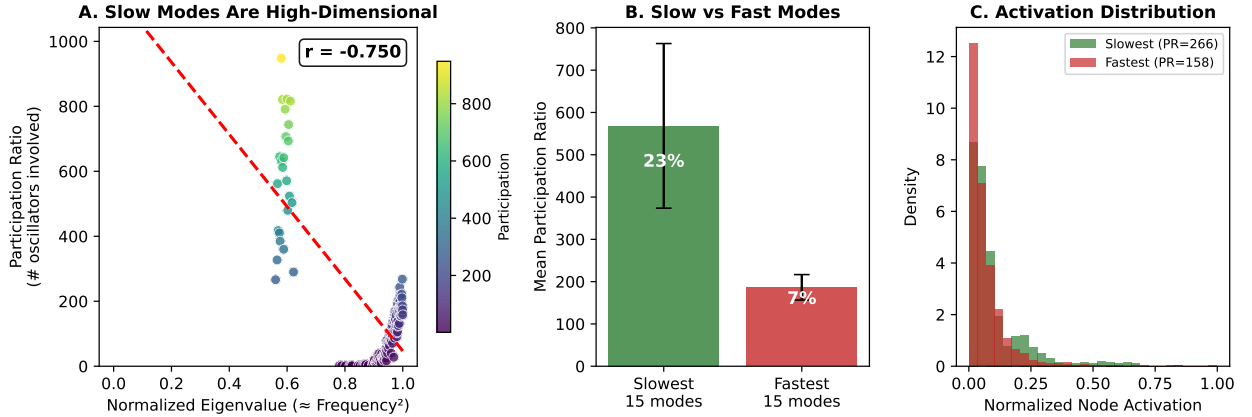

Figure 1: **Slow modes are geometrically high-dimensional.** (A) Participation ratio decreases with eigenvalue ($r = -0.75$). (B) Mean participation for slowest vs fastest modes shows 3-fold difference. (C) Activation distributions: slow modes spread activity broadly.
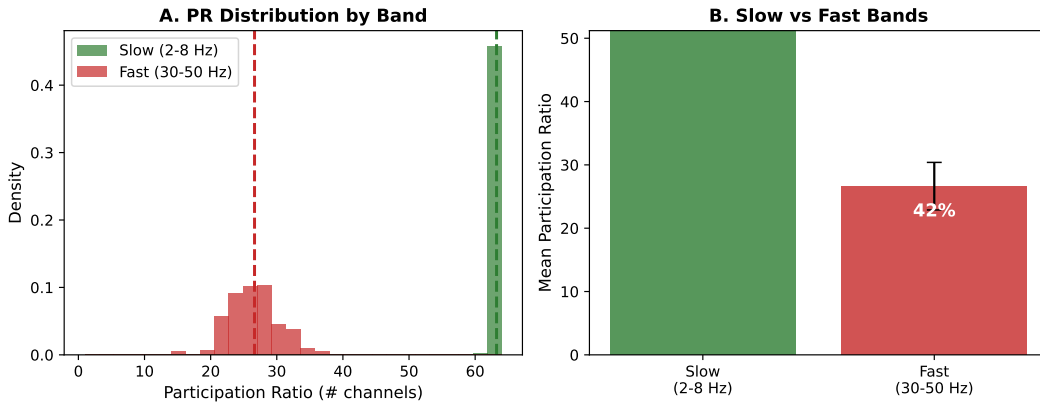

Figure 2: **Synthetic validation confirms PR metric.** (A) PR distributions for slow (2–8 Hz) versus fast (30–50 Hz) bands in synthetic multi-channel data. (B) Mean PR: slow band engages 99% of channels; fast band engages 42%. This 2.4-fold difference confirms that the metric correctly identifies global versus local activity when spatial structure is preserved.

3.2 Discrete Codes Emerge at $k = 2$

Figure 3 shows that code formation peaks at the critical bottleneck width $k = 2$ (ARI = 0.88). At $k = 1$, information is lost (ARI = 0.64). At $k \geq 3$, discretisation pressure diminishes and codes become more continuous (ARI = 0.85–0.87).

The critical $k = 2$ reflects a topological constraint: the input categories are distinguished by phase relationships (cyclic, S^1 topology). Embedding a circle requires exactly 2 dimensions; 1D is insufficient, 3D is redundant.
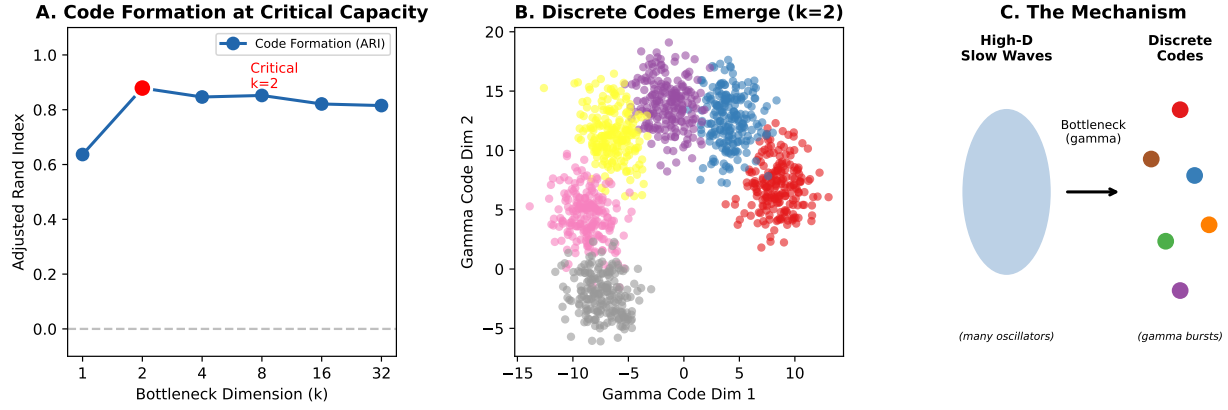

Figure 3: **Discrete codes emerge at critical capacity.** (A) Code formation (ARI) peaks at $k = 2$, reflecting the S^1 topology of the phase-defined categories. While $k = 3$ is topologically redundant for static embedding, Figure 4 shows it is dynamically essential for non-intersecting trajectories. (B) Bottleneck codes at $k = 2$ form six distinct clusters. (C) Schematic of compression mechanism.

3.3 Self-Reference Requires $k \geq 3$

Figure 4 demonstrates collision dynamics. The Liar's Paradox trajectory produces 1511 self-intersections when confined to 2D (the system cannot distinguish "going TRUE→FALSE" from "returning FALSE→TRUE"). In 3D, the trajectory forms a helix with zero self-intersections—the system can represent the *process* of the paradox without confusion.

4 Discussion

4.1 The Frequency Hierarchy

These results suggest that cortical frequency bands implement a cascade of dimensional bottlenecks:

- **Slow oscillations (delta, theta)**: Maintain the high-dimensional volumetric substrate. Many oscillators participate coherently, providing the "canvas" for computation.

- **Beta oscillations ($k \approx 3$)**: Intermediate compression. The manifold is constrained but remains "floppy"—continuous enough for analog manipulation, mental rotation, holding ambiguity.

- **Gamma oscillations ($k \approx 2$)**: Tight compression. Forces categorical commitment—symbols, decisions, assertions. Optimal for transmission but sacrifices nuance.

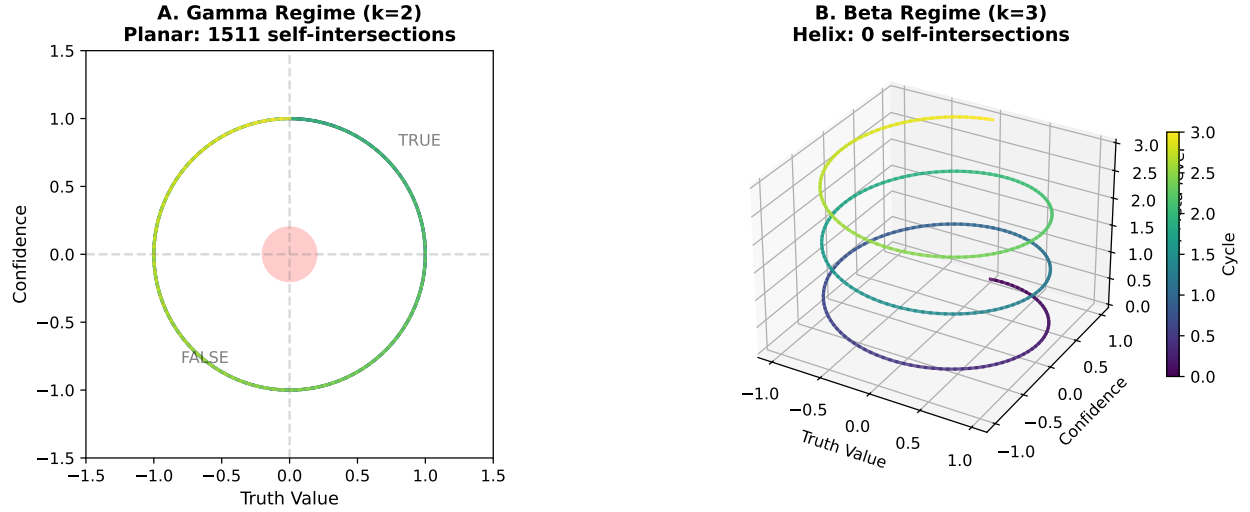The Liar's Paradox: Dimensional Requirements for Self-Reference

A. Gamma Regime (k=2)
Planar: 1511 self-intersections

B. Beta Regime (k=3)
Helix: 0 self-intersections

Figure 4: **Self-referential logic requires** $k \geq 3$. (A) In 2D, the paradox trajectory collides with itself every cycle. (B) In 3D, the trajectory spirals upward (helix), avoiding collision. Time/meta-level provides the escape dimension.

The brain may dynamically adjust bottleneck width via frequency shifts: increasing beta power to "loosen" the constraint when flexibility is needed; increasing gamma power to "tighten" when commitment is required.

4.2 Collision Dynamics and Meta-Cognition

The paradox simulation reveals a fundamental distinction:

- $k = 2$ (**Gamma**): Self-referential structures produce collisions. The system cannot stably represent "This statement is false." Attempting to do so produces oscillation, confusion, or collapse.

- $k \geq 3$ (**Beta**): The extra dimension allows trajectories to "lift" over themselves. The system can represent the *process* of the paradox—understand it—without being forced to resolve it.

This explains why we can *think about* paradoxes (beta, meta-cognition) but cannot *decide* them (gamma, assertion). The dimensional constraint determines what kinds of logic are representable.

4.3 Maturity and Long-Wavelength Stability

We speculate that the capacity to sustain $k \geq 3$ dynamics constitutes a geometric signature of cognitive and emotional maturity:

- **Immature/stressed cognition**: Defaults to $k = 2$. Everything is binary: good/bad, right/wrong, us/them. Contradictions are intolerable; ambiguity provokes anxiety.

- **Mature cognition**: Can sustain $k \geq 3$. Holds contradictions without forcing resolution. Tolerates ambiguity. Sees multiple perspectives simultaneously.

6

This geometric capacity likely tracks the biological maturation of the prefrontal cortex (PFC). The PFC is the primary generator of top-down beta oscillations (Miller et al., 2018) and is the last cortical region to fully myelinate, a process that continues into the mid-20s. The ability to sustain the "helical" $k \geq 3$ dynamics required for collision-free logic may be physically rate-limited by this development. The immature brain, lacking the myelinated bandwidth to sustain stable high-dimensional beta loops, falls back on earlier-developing, sensory-driven gamma circuitry ($k = 2$). Consequently, it defaults to a "planar" topology where paradoxes force immediate, binary resolution (impulsivity) rather than being held in suspension (cognitive control).

Long-wavelength oscillations provide the *temporal stability* needed for this capacity. Slow waves have long autocorrelation times—they change gradually, providing a stable backdrop against which complex, collision-free trajectories can unfold. When slow-wave power is compromised (stress, sleep deprivation, developmental immaturity, certain psychiatric conditions), the system loses this stability and collapses to categorical processing.

4.4 Cross-Frequency Coupling

The well-documented coupling between slow-wave phase and gamma amplitude (Canolty and Knight, 2010; Lisman and Jensen, 2013) may implement exactly this hierarchy. The slow oscillation defines the current position on the high-dimensional substrate; the gamma burst transmits a discrete "snapshot" of that position. The number of distinct gamma codes per slow cycle would be limited by $k = 2$ capacity, potentially explaining the 7±2 limit on working memory items (Lisman and Jensen, 2013).

4.5 Laminar and Bioelectric Connections

This architecture maps onto cortical laminar structure: deep layers (L5/6) with extensive horizontal connectivity support the slow, high-dimensional substrate; superficial layers (L2/3) with gamma-dominant activity implement the bottleneck.

More broadly, the motif of electric fields interacting with 2D surfaces recurs across biology: cell membranes, bioelectric gradients in morphogenesis (Levin, 2021), and cortical sheets all share this geometric configuration. The 2D surface may be a broadly useful architecture for transforming continuous volumetric dynamics into discrete signals.

4.6 Limitations and Measurement Requirements

While synthetic validation confirms the PR metric's utility (Figure 2), preliminary application to scalp EEG (64-channel recordings) yielded null results. This is expected: scalp EEG measures volume-conducted potentials that spatially blur the fine-grained geometric structure. The slow-wave versus fast-wave PR difference requires electrode spacing finer than the spatial scale of functional oscillator units. Cortical columns span ∼300–500 μm; resolving participation at this scale requires Utah-array density (∼400 μm pitch) or high-density ECoG. Standard ECoG grids (1 cm spacing) may still average over too many columns. This represents a clear experimental target: PR analysis on dense intracranial recordings during tasks requiring flexibility (beta-dominant) versus commitment (gamma-dominant).

The models presented here isolate geometric and information-theoretic aspects; they do not capture excitatory-inhibitory dynamics, conduction delays, or synaptic nonlinearities. Future work should test these predictions in biologically realistic spiking networks and empirical data with appropriate spatial resolution.

5   Conclusion

Cortical oscillations implement a dimensional hierarchy: slow waves maintain the high-dimensional analog substrate; beta provides intermediate "floppy" compression for manipulation; gamma enforces discrete symbol formation. The capacity to sustain $k \geq 3$ dynamics—to hold paradoxes without collision—may be a geometric signature of maturity. Long-wavelength stability provides the temporal substrate for collision-free cognition; its disruption forces the mind into rigid categorical processing.

Intelligence emerges from the controlled collapse of analog into digital. The canvas is slow; the brushstrokes are fast.

Data Availability

Code for all simulations is available at: `https://github.com/todd866/brainwavedimensionality`

References

Bastos, A. M., Vezoli, J., Bosman, C. A., Schoffelen, J.-M., Oostenveld, R., Dowdall, J. R., De Weerd, P., Kennedy, H., and Fries, P. (2015). Visual areas exert feedforward and feedback influences through distinct frequency channels. *Neuron*, 85(2):390–401.

Canolty, R. T. and Knight, R. T. (2010). The functional role of cross-frequency coupling. *Trends in cognitive sciences*, 14(11):506–515.

Levin, M. (2021). Bioelectric signaling: Reprogrammable circuits underlying embryogenesis, regeneration, and cancer. *Cell*, 184(6):1971–1989.

Lisman, J. E. and Jensen, O. (2013). The theta-gamma neural code. *Neuron*, 77(6):1002–1016.

Lundqvist, M., Rose, J., Herman, P., Brincat, S. L., Buschman, T. J., and Miller, E. K. (2016). Gamma and beta bursts underlie working memory. *Neuron*, 90(1):152–164.

Miller, E. K., Lundqvist, M., and Bastos, A. M. (2018). Working memory 2.0. *Neuron*, 100(2):463–475.